RSC Advances

PAPER

View Article Online
View Journal | View Issue

Cite this: *RSC Adv.*, 2021, **11**, 3732

N-type thermoelectric Ag_8SnSe_6 with extremely low lattice thermal conductivity by replacing Ag with Cu†

Chao Yang, [ab] Yong Luo, *[a] Xie Li[b] and Jiaolin Cui *[b]

Argyrodite family compounds inherently possess low lattice thermal conductivity (κ_L) due to the liquid-like behavior of cations and the intimate interplay among mobile ions. Hence, they have become the focus of discussion in thermoelectrics recently. However, the major bottleneck for further improvement of their thermoelectric (TE) performance is their low carrier concentration. In this work, we take an advantage of the unique structure of Ag_8SnSe_6, in an attempt to further reduce the lattice part (κ_L) while at the same time improve their electrical property. The results show that the κ_L value reduces from 0.17 W K^{-1} m^{-1} to 0.12 W K^{-1} m^{-1} when Ag is substituted for Cu through induced point defects and lattice distortion and that the power factor (PF) increases from 4.1 μW cm^{-1} K^{-2} to 4.4 μW cm^{-1} K^{-2} at 645 K after enhancing the Seebeck coefficients. Finally, the maximum *ZT* value of ~0.85 is attainted for $Ag_{7.95}Cu_{0.05}SnSe_6$ at 645 K, an increase by a factor of 1.3 compared to that of the pristine Ag_8SnSe_6. This result demonstrates that the replacement of Ag by Cu in Ag_8SnSe_6 is an effective way to improve its TE performance.

Received 12th December 2020
Accepted 11th January 2021

DOI: 10.1039/d0ra10454j

rsc.li/rsc-advances

1 Introduction

A growing number of researchers direct their attention to thermoelectric (TE) applications as the TE materials can directly convert heat to electricity without moving parts or emitting greenhouse gases.[1–4] The TE performance can generally be characterized by the dimensionless figure of merit *ZT* ($ZT = T\alpha^2\sigma/\kappa$), where *T*, α, σ and κ are the absolute temperature, Seebeck coefficient, electrical conductivity, and total thermal conductivity which is the sum of lattice (κ_L) and electronic (κ_e) parts mainly. In order to enhance the *ZT* value, one should boost $\alpha^2\sigma$ called the power factor (PF), which is associated with electrical transport properties, and reduce κ simultaneously. However, it is still challenging to improve the TE performance significantly because of the interdependency among the three parameters (α, σ and κ_e).

In the past two decades, many strategies have been developed, such as the band engineering near the Fermi level[5–12] and nanomicrostructure engineering.[13–15] The former aims at optimizing the electronic structure and the latter strengthening phonon scattering by introducing lattice distortion and nanostructures. Additionally, some materials with very low intrinsic thermal conductivity has been attracting much attention, due to either resonant bonding,[16,17] the loosely bonded atoms in atomic voids with rattling[18] or "liquid-like behavior".[19,20] The aforementioned strategies can generally be realized by off-stoichiometry in composition and element doping.[6,13] Although the carrier concentration can slightly be tuned *via* composition engineering[21] due to the presence of thermodynamic equilibrium state of the material, it is found that isoelectronic substitution seems more effective in reducing the lattice part κ_L and modulating the carrier concentration simultaneously for semiconductors with weak chemical bonds.[22,23] For example, the substitution of Cu on Ag in Ag_9GaSe_6 or Ag for Cu in Cu_8GeSe_6 can decrease κ_L without degrading the electrical property.[24,25] Because of the different features between the Cu–Se and Ag–Se chemical bonds[26] (see Fig. S1†), the carrier concentrations of Cu-contained binary chalcogenides are usually about one order higher in magnitude than those of Ag-contained counterparts,[26–31] and the same situation applies to the ternary argyrodite family compounds.[24,32–35] This gives us inspirations that the carrier concentration can be enhanced by isoelectronic substitution of elements in terms of their chemical bonds.

In addition, guided by the "phonon–liquid electron–crystal (PLEC)" concept proposed by Liu *et al.*,[36] argyrodite-type compounds has drawn significant attention in thermoelectrics in recent years. This material has a general formula $A_{(12-n)/m}{}^{m+}B^{n+}X_6{}^{2-}$ (A^{m+} = Li^+, Cu^+, or Ag^+, B^{n+} = Ga^{3+}, Si^{4+}, Ge^{4+}, Sn^{4+}, p^{5+}, or As^{5+}, and X = S, Se, or Te). Due to their complex crystal structures and weakly bonded Ag or Cu atoms, the argyrodite-type compounds exhibit intrinsically low κ_L. For example, Lin *et al.* reported that the acoustic phonons of argyrodite Ag_9GaSe_6 has an extremely low cutoff frequency (only ~0.5 THz), which makes its κ_L as low as ~0.15 W m^{-1} K^{-1} in the entire

[a]School of Chemical Engineering & Technology, China University of Mining and Technology, Xuzhou, 221116, China

[b]School of Material & Chemical Engineering, Ningbo University of Technology, Ningbo, 315016, China. E-mail: cuijiaolin@163.com

† Electronic supplementary information (ESI) available. See DOI: 10.1039/d0ra10454j

temperature range. As a result, a peak figure of merit ZT ($ZT \sim 1.5$) is attained at 850 K.[34] Another similar compound Cu_8GeSe_6 has a low κ_L value of 0.2 W m^{-1} K^{-1} and ZT value as high as 1.0.[24] For the Ag_8SnS_6 compound, it is reported that lattice part κ_L is 0.31–0.61 W m^{-1} K^{-1},[37] much higher than those observed in Ag_9GaSe_6 and Cu_8GeSe_6 and that the recorded ZT value is only 0.8. Therefore, it is highly likely to improve the TE performance of Ag_8SnS_6 if its κ_L value can be further reduced.

In this work, we replace Ag with Cu in Ag_8SnSe_6, in an attempt to tune the carrier concentration and reduce the lattice part κ_L by introducing point defects. It is found that there are two diverse effects on κ_L: the first one is the increased point defects and lattice distortion upon the replacement of Ag by Cu, which, as a result, strengthens the phonon scattering; the second one is that this replacement weakens the "liquid-like behavior". Due to the higher bond energy of Cu–Se (255 kJ mol^{-1}) than that of Ag–Se (210 kJ mol^{-1}) (Fig. S1†) in chalcogenide glasses,[38] the thermal conductivities increases. Consequently, we observed a low lattice part ($\kappa_L \sim 0.12$ W m^{-1} K^{-1}) at 645 K. This κ_L value, which is lower than those of Nb-doped and extra Sn-added Ag_8SnSe_6,[23,39] is mainly responsible for the improvement in TE performance with the highest ZT value of 0.85. This work proves that the substitution of Cu on Ag in Ag_8SnSe_6 can effectively improve its TE performance.

2 Experimental

2.1 Sample preparation

The four high-purity elements (with the purity > 99.999%, Emei Semicon. Mater. Co., Ltd. Sichuan, CN) were weighted in stoichiometric ratio and sealed in evacuated quartz ampoules to synthesize polycrystalline samples of $Ag_{8-x}Cu_xSnSe_6$ (x = 0, 0.025, 0.05, 0.075 and 0.1). The mixtures of the four elements were melted at 1273 K for 48 h and quenched in cold water. Subsequently, the ingots were annealed at 527 K for 72 h and then cooled down to room temperature (RT) in furnace.

The ingots were then ball milled for 5 h at a rotation rate of 350 rpm in stainless steel bowls that contain benzinum before drying. The dried powders were loaded into graphite dies and sintered using the spark plasma sintering apparatus (SPS-1030) at 600 K under a pressure of 55 MPa. The obtained pellets have a density about 98% of the theoretical one.

The obtained samples were ground into square-crossed long bars with in sizes of about 2 × 3 × 10 mm^3 and 2 × 2 × 7 mm^3 for electrical property and Hall coefficients measurements respectively and coin-shaped disks of φ10 × 1.5 mm^2 for thermal diffusivity measurement.

2.2 Physical property measurements

The electrical transport properties including Seebeck coefficient (α) and electrical conductivity (σ), and the thermal diffusivity (D) at a temperature ranging from ∼RT to ∼650 K were measured by using ZEM-3 (ULVAC-RIKO, Japan) and TC-1200RH (ULVAC-RIKO, Japan). The thermal conductivities (κ) were calculated from the formula $\kappa = \rho C_p D$, where ρ is the density of pellet measured by the Archimedes method and C_p is the estimated heat capacity presented by Li *et al.*[40] The electronic contributions (κ_e) is expressed by the Wiedemann–Franz (W–F) relation, $\kappa_e = L_o \sigma T$, where L_o is the Lorenz number, estimated using the formula $L_o = 1.5 + \exp(-|\alpha|/116)$[24] (where L_o is in 10^{-8} W Ω K^{-2} and $|\alpha|$ in μV K^{-1}).

Hall coefficients (R_H) were measured by using a four-probe configuration in a system (PPMS, Model-9) with a magnetic field up to ±5 T. The Hall mobility (μ) and carrier concentration (n_H) were calculated according to the formulae $\mu = |R_H|\sigma$ and $n_H = 1/(eR_H)$ respectively, where e is the electron charge.

The TE figure of merits (ZTs) were calculated by the three parameters mentioned above with a total uncertainty of ∼18.0%.

2.3 Compositions and structural analyses

The X-ray diffraction (XRD) patterns of $Ag_{8-x}Cu_xSnSe_6$ (x = 0, 0.025, 0.05, 0.075 and 0.1) were obtained on an X-ray diffractometer (XRD, D8 Advance) instrument operated at 50 kV and 40 mA (Cu Kα radiation, λ = 0.15406 nm) in the 2θ range from 10° to 110° with a step size of 0.02°, and the XRD patterns were refined by utilizing a X'Pert Pro, PANalytical code. The lattice constants a, b and c were directly attained from the Rietveld refinement on the XRD patterns with an error less than 0.3–0.4%. A high-resolution transmission electron microscopy (HRTEM; JEM-2010F) operated at 200 kV was employed to observe the microstructures of $Ag_{7.95}Cu_{0.05}SnSe_6$.

The absorption coefficient measurements and UV absorption spectra analyses for the powders were carried out using a PerkinElmer Lambda 950 UV-VIS-NIR spectrophotometer.

The phase transition was studied by a differential scanning calorimeter (DSC), which was conducted in a Netzch STA 449 F3 Jupiter equipped with a TASC414/4 controller with a heating rate of 5 K min^{-1} under an argon atmosphere.

3 Result and discussion

3.1 Compositions and structures

The scanning electron microscopy (SEM) image of the surface-polished sample $Ag_{7.95}Cu_{0.05}SnSe_6$ was observed, and only a few pores can be seen, as shown in Fig. S2a (ESI).† From the EDS patterns and mappings of the elements (Fig. S2b–f†), there are slight segregations of the elements (Ag, Cu, Sn and Se) within the grains, indicating that the elements are not distributed uniformly.

The X-ray diffraction patterns of $Ag_{8-x}Cu_xSnSe_6$ (x = 0, 0.025, 0.05, 0.075 and 0.1) are summarized in Fig. 1a. The diffraction peaks of all the samples can be well indexed to the low-temperature β-phase (space group: $Pmn2_1$, ICSD #95093) with no impurities identified. Besides, the main diffraction peaks shift to the high angle site as the Cu content increases (Fig. 1b), indicating a shrinking in the crystal structure. This is due to the smaller ionic radius of Cu^+ (0.77 Å) than that of Ag^+ (1.15 Å) and can be further verified by the decreased lattice parameters (a, b, c), as shown in Fig. 1c. The parameter c reduces remarkably while a and b exhibit only a slight decreasing tendency. Besides, they all decrease linearly, conforming to Vegard's law. This suggests that element Cu is fully incorporated into the Ag_8SnSe_6 matrix.

In order to check the phase transition in the measured temperature range, the XRD analysis to the sample Ag_8SnSe_6 at

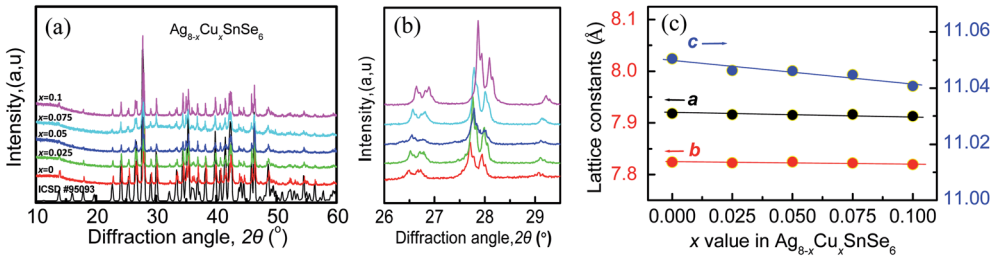

Fig. 1 (a) X-ray diffraction patterns of the $Ag_{8-x}Cu_xSnSe_6$ ($x = 0$, 0.025, 0.05, 0.075 and 0.1) powders; (b) close-up view of the patterns between 26–30°; (c) lattices constants (*a*, *b*, *c*) as a function of *x* value.

various temperatures (300 K, 373 K, 450 K and 600 K) is carried out. The results are presented in Fig. 2a. It is noted that the material undergoes a phase transition from the orthorhombic β-phase (ICSD #95093) to the cubic γ-phase (PDF #19-1133) at ~370 K. The low-temperature β-phase is widely considered as a non-superionic phase while the high-temperature γ-phase is a superionic one with highly mobile silver ions. At 450 K, all of the $Ag_{8-x}Cu_xSnSe_6$ ($x = 0$, 0.025, 0.05 and 0.075) materials are indexed to cubic γ-Ag_8SnSe_6 (PDF #19-1133) without any impurities identified (see Fig. 2a and b).

Generally, phase transition is unfriendly to practical application for thermoelectric devices because of the thermal expansion stress created between different phases.[23,41] Therefore, it is necessary to reduce the phase transition temperature (T_c) and extend the temperature range in application. In this work, it is observed that T_c decreases with an increase in the content of Cu, as shown in Fig. 3a, and the detailed relation of T_c to the *x* value is summarized in Fig. 3b. The depression of T_c can be ascribed to the increase in the configurational entropy (ΔS) upon the incorporation of Cu into $Ag_{8-x}Cu_xSnSe_6$,[42] which can be determined by the following formula:[43,44]

$$\Delta S = -k_B \sum_{i=1}^{N} x_i \ln(x_i) \quad (1)$$

where k_B is the Boltzmann constant, x_i the composition of each species, and $\sum_{i=0}^{N} x_i = 1$.

It is observed that, the calculated configurational entropy (ΔS) of $Ag_{8-x}Cu_xSnSe_6$ gradually increases with the *x* value rising, as manifested in Fig. 3c. This indicates that the increased ΔS is mainly responsible for the depression of T_c. Such a phenomenon has been reported in many works.[45–47] For example, the incorporation of $AgSbSe_2$ in GeSe increases the configurational entropy (ΔS) and promotes the formation of a high symmetry phase, thus improving the TE performance.[48] Besides, the highly tunable entropy caused by atomic substitutions can strongly scatter phonons and reduce the lattice thermal conductivities.[33]

The absorption coefficient (A) as a function of photon energy ($h\nu$) is presented in Fig. 4a, and the experimentally determined bandgap (E_g) using a full spectra $(Ah\nu)^2$ ($h\nu$) is shown in Fig. 4b. It is observed that the optical band gap (E_g) of intrinsic Ag_8SnSe_6 is ~0.8 eV, agreeing well with the previously reported values.[11,39] After Cu is added to the Ag_8SnSe_6, E_g decreases from 0.8 at $x = 0$ to 0.73 at $x = 0.1$, as shown in Fig. 4c, indicating a narrowing in the bandgap. This is critical because the drop in E_g allows the thermal excitation of electrons to the conduction bands to be easier, thus increasing the carrier concentration, and improving the transport properties.[39] The presence of the another peak with an energy of 0.65 eV in absorption coefficient might be related to the intravalence-band transition (split-off band to heavy- or light hole band).[49]

3.2 Transport properties and TE performance

In order to have a deep understanding of the electronic transport properties upon doping, the Hall coefficients (R_H) at room temperature (RT) are measured, and the Hall carrier concentration (n_H) and mobility (μ) are calculated (Fig. 5a). It is

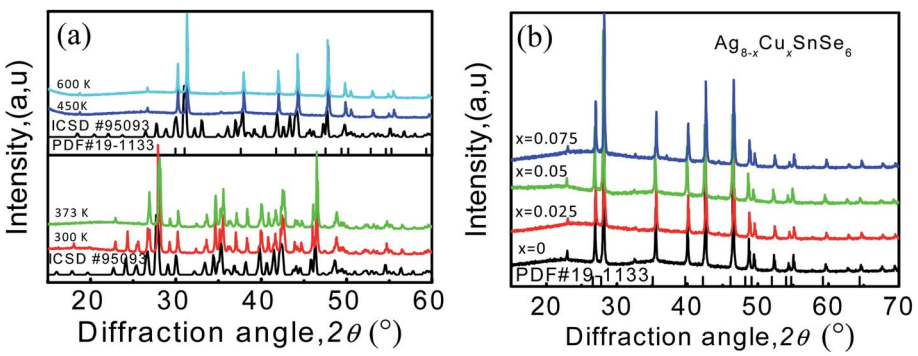

Fig. 2 (a) PXRD patterns of Ag_8SnSe_6 at 300 K, 373 K, 450 K and 600 K; (b) PXRD patterns of $Ag_{8-x}Cu_xSnSe_6$ ($x = 0$, 0.025, 0.05, 0.075) at 450 K.

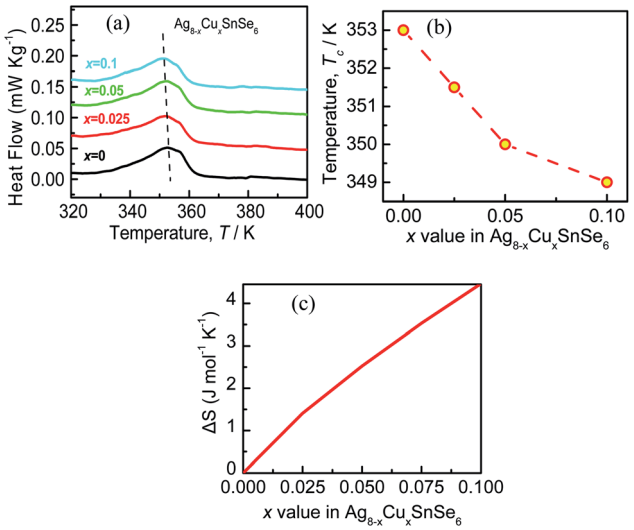

Fig. 3 (a) Measured DSC curves of $Ag_{8-x}Cu_xSnSe_6$ (x = 0, 0.025, 0.05 and 0.1) from 320 K to 400 K; (b) the phase transition temperature (T_c) as a function of x value; (c) calculated configurational entropy (ΔS) of $Ag_{8-x}Cu_xSnSe_6$.

observed that the n_H value enhances from 1.93×10^{16} cm^{-3} at x = 0 to 8.61×10^{16} cm^{-3} at $x = 0.1$, comparable to that reported by Acharya *et al.*[50] Usually, the mobility μ decreases because of ionized impurity and carrier scattering.[51–53] However, the mobility μ in the present work is laying in the range of 1.17×10^2 cm^2 V^{-1} s^{-1} and 1.34×10^2 cm^2 V^{-1} s^{-1} when x value increases from 0 to 0.075 and remains almost unchanged, and then it drops as the x value exceeds 0.075. Such a phenomenon, which is also observed in the $Zn_{1-x}Al_xO$ system,[54] is attributed to a novel micro/nano-structure that provides a favorable crystalline framework for rapid electron transfer. In this work, we speculate that the almost unchanged mobility at $x \leq 0.075$ is

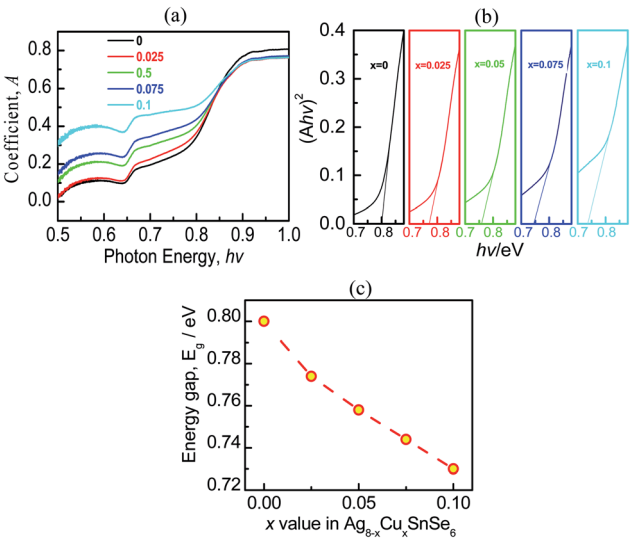

Fig. 4 (a) Absorption coefficient (A) as a function of photon energy ($h\nu$) for different x values; (b) experimentally determined bandgap using full spectra $(Ah\nu)^2$ ($h\nu$), based on the measured coefficients (A); (c) bandgap (E_g) as a function of x value.

due to the limited change of the effective mass (m^*), as shown in Fig. 5b, as all the Seebeck coefficients at RT follow the Pisarenko relation when $m^* = 0.055m_e$, determined by the eqn (2), assuming that the present materials are degenerate semiconductors (single parabolic band, energy-independent scattering approximation).[55] Only the α values at $x = 0.1$ are much high above the Pisarenko relation line.

$$a = \frac{8\pi^2 k_B^2}{3eh^2} m^* T \left(\frac{\pi}{3n}\right)^{\frac{2}{3}} \quad (2)$$

Here, α is Seebeck coefficient and m^* is the effective mass of the carrier.

The drop of μ in $x = 0.1$ is probably attributed to the increased effective mass and the introduced point defects that play a dominant role in impeding the carrier mobility.[56]

The temperature-dependent electrical transport properties are depicted in Fig. 6, where the Seebeck coefficients (α) are demonstrated in Fig. 6a. The Seebeck coefficients of all the samples are negative throughout the entire temperature range, indicative of the n-type conduction behavior. The systematic decrease in $|\alpha|$ with x values increasing below 353 K (phase transition temperature) is in line with the increased carrier concentration, as was observed in Cu_7PSe_6 compound.[45] On the other hand, the composition dependence of the $|\alpha|$ for the samples doped with Cu becomes complicated. A similar appearance also happens to the electrical conductivities, as shown in Fig. 6b, in which the electrical conductivities of doped Ag_8SnSe_6 are higher at a low temperature but lower at the elevated temperatures. This may be related to the structural transformation from $Pmn2_1$ to $F\bar{4}3m$. Finally, the highest power factor of 4.35 μW cm^{-1} K^{-2} is attained at 645 K in $Ag_{7.95}Cu_{0.05}SnSe_6$, slightly higher than that of the pristine Ag_8SnSe_6 (4.11 μW cm^{-1} K^{-2}).

The temperature dependent of the total thermal conductivities (κ) and the lattice thermal conductivities (κ_L) are displayed in Fig. 6c and d. The κ value decreases until the phase transition temperature (T_c), and then increases with the temperature increasing, similar to those reported in ref. [57–60]. Over the entire temperature range, the total thermal conductivities (κ) are very low, within the scale of 0.15–0.45 W K^{-1} m^{-1}. This value approaches the amorphous limit, based on the Cahill model described below:

$$k_{min} = \left(\frac{\pi}{6}\right)^{\frac{1}{3}} k_B V^{-\frac{2}{3}} \sum_i v_i \left(\frac{T}{\Theta_i}\right)^2 \int_0^{\Theta_i/T} \frac{x^3 e^x}{e^x - 1} dx \quad (3)$$

$$\Theta_i = \left(\frac{v_i h}{2\pi k_B}\right)\left(\frac{6\pi^2}{V}\right)^{1/3} \quad (4)$$

Here, k_B and V are Boltzmann constant and the average volume per atom, respectively, v_i the sound velocity of the three sound modes (one longitudinal mode and two transverse modes) and Θ_i the corresponding cutoff frequency for these modes. The calculated glassy limit κ_{min} is 0.44 W K^{-1} m^{-1}, which is revealed in the dotted line illustrated in Fig. 6c. However, in terms of calculation, we surprisingly observed that the measured κ values are even lower than that estimated in the measuring

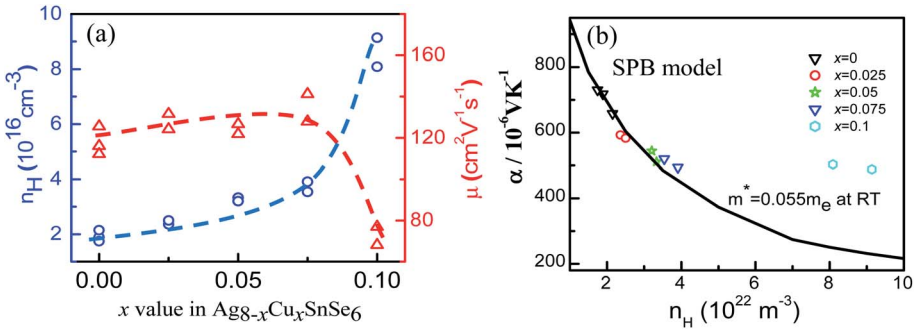

Fig. 5 (a) Hall carrier concentration (n_H) and mobility (μ) as a function of x value; (b) experimentally determined Seebeck coefficients (α) at corresponding Hall carrier concentrations. The solid line represents the Pisarenko relation at RT. It is observed that the Seebeck coefficients at $x = 0.1$ are much high above the Pisarenko line.

temperature range (300–650 K). This abnormal appearence is also observed in the Cu_7PSe_6 (ref. [44] and [61]) and Cu_2X (X = S, Se, Te)[62–64] systems. Such a phenomenon can be regarded as a softening or loss in some phonon modes, and it makes no contributions to the thermal conductivity.

In addition, most of the samples gives lower thermal conductivities than that of the pristine sample at high temperatures. In addition to that, the κ value at high temperatures reduces with the x value increasing until at $x = 0.05$, after which it enhances continuously. The minimum κ_{min} value is 0.34 W K^{-1} m^{-1} at ~650 K for the sample at $x = 0.05$. It is considered that the reduction of κ at elevated temperatures arises mainly from two parts: one is the degraded electrical conductivity (κ_e) with an elevating temperature, as shown in Fig. 6d, and the other is the reduction of lattice part κ_L resulting from strongly intensified phonon scattering by point defects. The κ_L is attained by subtracting the κ_e from κ, where κ_e can be calculated *via* the Wiedemann–Franz law $\kappa_e = L_oT\sigma$, and Lorenz factor (L_o) is estimated by the measured Seebeck coefficients.

Generally, the temperature dependence of the lattice part (κ_L) is quite different from that of the total κ, as the κ_L value increases with temperature at $T < 550$ K and drops at high temperatures. This presence can be seen in many other Ag_8SnSe_6 compounds,[23,39] but its nature is hard to unravel yet at the moment. One of the possible explanation is that above 550 K the electrical conductivities (σ) have a sharp increase (Fig. 6b), which implies that the carrier concentration increases significantly, thus enhancing the phonon scattering of the carriers and reducing the κ_L. The another reason is the creation of the point defect Cu_{Ag} upon Cu substitution on Ag, thus enhancing the phonon scattering at high temperatures. On the other hand, the κ_L above T_c first decreases until at $x = 0.05$ and then increases with an increase of the x value, indicating the presence of other scattering mechanisms, in addition to the scattering on the points defects. Since the highly mobile silver or copper ions in the argyrodite compounds are distributed in disorder at elevated temperatures due to relatively weak chemical bonding between Ag–Se or Cu–Se,[65] the superionic argyrodites generally have inherent ultra-low lattice

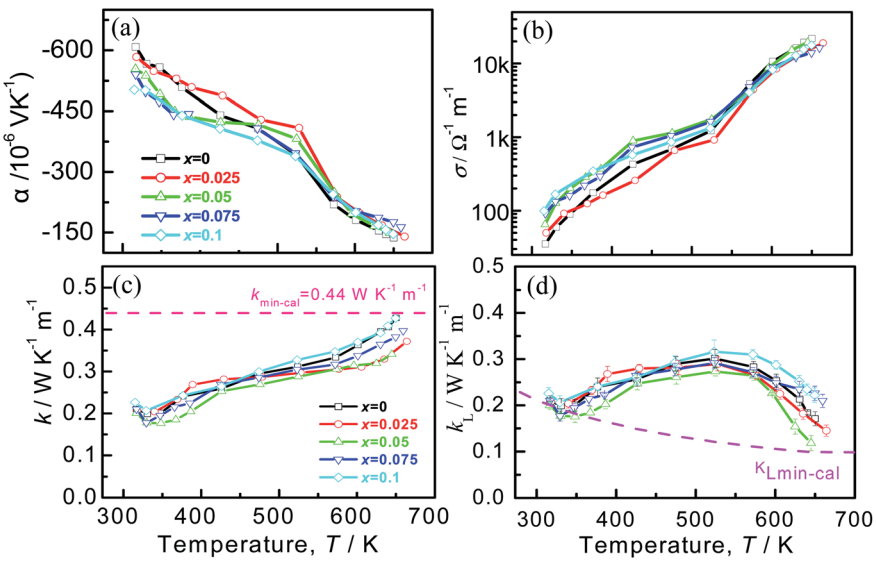

Fig. 6 Electrical and thermal properties of $Ag_{8-x}Cu_xSnSe_6$ (x = 0, 0.025, 0.05, 0.075, 0.1). (a) Seebeck coefficients (α) as a function of temperature; (b) electrical conductivities (σ) as a function of temperature; (c) total thermal conductivities (κ) as a function of temperature; (d) lattice thermal conductivities (κ_L).

thermal conductivity because of liquid-like behavior of cations in a relatively larger unit cell. On the other hand, the Cu–Se bond is stronger compared to Ag–Se in most compounds (see Fig. S1†), as mentioned above. The stronger the bonding is, the higher the sound velocity.[23,66] In this regard, there is a dual effect that regulates κ_L: one is point defects formed by cation substitution, which reduces the lattice part κ_L,[37] and the other is the introduction of stronger Cu–Se bond than Ag–Se, which increases the κ_L value. That is why we observed the minimum $\kappa_L \sim 0.12$ W K^{-1} m^{-1} at $x = 0.05$ and 645 K.

In order to elucidate the ultra-low lattice part in the high temperatures at $x = 0.05$, we estimate the κ_L by using the Slack and Morelli model[67,68] given below, where the interactions among the phonons themselves *via* anharmonic Umklapp processes are only concerned.

$$k_L = \frac{AM_{av}\Theta^3\delta}{\gamma^2 n^{\frac{2}{3}}T} \quad (5)$$

$$A = \frac{2.43 \times 10^{-8}}{1 - \frac{0.514}{\gamma} + \frac{0.228}{\gamma^2}} \quad (6)$$

Here γ is the Gruneisen constant ($\gamma = 2.4$)[11] and $A = 2.94 \times 10^{-8}$. $M_{av} = 97.03$ is the average atom mass in the atomic mass unit, δ^3 the volume per atom, Θ (163 K)[11] the Debye temperature and n ($n = 30$) the number of atoms in the primitive unit cell. In terms of the estimation above, we obtain the curve of estimated κ_L values with temperature, as shown in Fig. 6d in dark cyan line, where it is observed that the estimated $\kappa_{L,min}$ value decreases as the temperature rise and it is only $\sim$0.1 W K^{-1} m^{-1} at 645 K, very close to the measured minimum value ($\sim$0.12 W K^{-1} m^{-1}). This confirms that the replacement of Ag by Cu can effectively reduce the lattice part κ_L.

Combined with the three parameters (α, σ, κ), we estimate the *ZT* values that are shown in Fig. 7. The highest *ZT* value of $\sim$0.85 is achieved for $Ag_{7.95}Cu_{0.05}SnSe_6$ at 645 K, which is about 30% higher than that of the pristine Ag_8SnSe_6. It is noted that the reported *ZT* value (above unity) by other researchers is attained at 800 K or even higher.[11,23,39,40] If we compare the TE performance at 645 K, the present *ZT* value is comparable to or a little higher than those from others. Since above 645 K the samples failed holding their shapes during the electrical property measurement in our work, we have no results above 645 K.

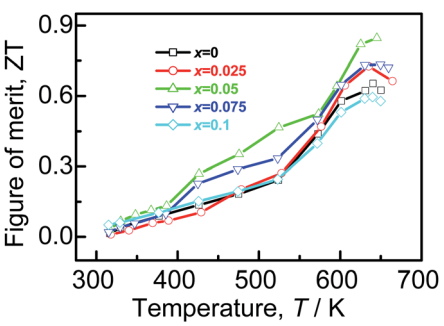

Fig. 7 TE figure of merit (*ZT*) as a function of temperature.

4 Conclusions

In this work, a series of argyrodite type compounds $Ag_{8-x}Cu_xSnSe_6$ ($x = 0.025$, 0.05, 0.075 and 0.1) have been prepared and their TE performance examined. The results reveal that the lattice thermal conductivities reduces significantly without degradation of the electronic transport properties. The minimum $\kappa_L \sim 0.12$ W K^{-1} m^{-1} is attained at $x = 0.05$ at 645 K, in a good agreement with that (0.1 W K^{-1} m^{-1} at 645 K) estimated by using the Slack and Morelli model. Consequently, the maximum *ZT* value of $\sim$0.85 is achieved for $Ag_{7.95}Cu_{0.05}SnSe_6$ at 645 K, comparable to or a little higher than those in the other Ag_8SnSe_6 samples at the corresponding temperature.

Conflicts of interest

There are no conflicts of interest to declare.

Acknowledgements

This work is supported by the National Natural Science Foundation of China (51671109, 51171084).

References

1 L. E. Bell, Cooling, *Science*, 2008, **321**, 1457–1461.
2 I. Petsagkourakis, K. Tybrandt, X. Crispin, I. Ohkubo, N. Satoh and T. Mori, *Sci. Technol. Adv. Mater.*, 2018, **19**, 837–862.
3 M. T. Dunham, T. J. Hendricks and K. E. Goodson, *Adv. Heat Transfer*, 2019, **51**, 299–350.
4 N. Nandihalli, C. Liu and T. Mori, *Nano Energy*, 2020, **78**, 105186.
5 V. Dinnocenzo, A. R. S. Kandada, M. D. Bastiani, M. Gandini and A. Petrozza, *J. Am. Chem. Soc.*, 2014, **136**, 17730.
6 R. A. Orabi, N. Mecholsky, J. Hwang and W. Kim, *Chem. Mater.*, 2016, **28**, 5b04365.
7 A. Topp, J. M. Lippmann, A. Varykhalov, V. Duppel, B. V. Lotsh, C. R. Ast and L. M. Schoop, *New J. Phys.*, 2016, **18**, 125014.
8 G. Tan, F. Shi, S. Hao, C. Hang, L. D. Zhao, C. Uher, C. Wolverton, V. P. Dravid and M. G. Kanatzidis, *J. Am. Chem. Soc.*, 2015, **137**, 5100.
9 Z. W. Chen, Z. Z. Jian, W. Li, Y. J. Chang, B. H. Ge, R. Hanus, J. Yang, Y. Chen, M. X. Huang, G. J. Snyder and Y. Z. Pei, *Adv. Mater.*, 2017, **29**, 1606768.
10 S. Y. Wang, Y. X. Sun, J. Yang, B. Duan, L. H. Wu, W. Q. Zhang and J. H. Yang, *Energy Environ. Sci.*, 2016, **9**, 3436.
11 M. Jin, S. Q. Lin, W. Li, Z. W. Chen, R. B. Li, X. H. Wang, Y. X. Chen and Y. Z. Pei, *Chem. Mater.*, 2019, **31**, 2603.
12 H. Wang, Y. Z. Pei, A. D. Lalonde and G. J. Snyder, *Thermoelectric Nanomaterials*, 2013, vol. 182, pp. 3–32.
13 S. Gorsse, P. B. Pereira, R. Decourt and E. Sellier, *Chem. Mater.*, 2010, **22**, 988.
14 S. J. Hong and B. S. Chun, *Mater. Res. Bull.*, 2003, **38**, 599.

15 T. H. An, S. M. Choi, W. S. Seo, C. Park, I. H. Kim and S. U. Kim, *Jpn. J. Appl. Phys.*, 2013, **52**, 10MC11.
16 S. Lee, K. Esfarjani, T. Luo, J. Zhou, Z. Tian and G. Chen, *Nat. Commun.*, 2014, **5**, 4525.
17 W. Zhang, N. Sato, K. Tobita, K. Kimura and T. Mori, *Chem. Mater.*, 2020, **32**, 5335–5342.
18 G. A. Slack, *CRC Handbook of Thermoelectric*, 1995, p. 407.
19 Z. X. Zhang, K. P. Zhao, T. Wei, P. F. Qiu, L. D. Chen and X. Shi, *Energy Environ. Sci.*, 2020, **13**, 3307–3329.
20 T. Mao, P. F. Qiu, J. Liu, X. L. Du, P. Hu, K. P. Zhao, D. D. Ren, X. Shi and L. D. Chen, *Phys. Chem. Chem. Phys.*, 2020, **22**, 7374–7380.
21 S. Lee, J. A. Bock, S. T. Mckinstry and C. A. Randall, *J. Eur. Ceram. Soc.*, 2012, **32**, 3971.
22 P. Ying, X. Li, Y. Wang and J. Yang, *Adv. Funct. Mater.*, 2017, **27**, 1604145.
23 W. Li, S. Q. Lin, B. H. Ge, J. Yang, W. Q. Zhang and Y. Z. Pei, *Adv. Sci.*, 2016, **3**, 1600196.
24 B. B. Jiang, P. F. Qiu, E. Eikeland, H. Y. Chen, Q. F. Song, D. D. Ren, T. S. Zhang, J. Yang, B. B. Iversen, X. Shi and L. D. Chen, *J. Mater. Chem. C*, 2017, **5**, 943.
25 X. Y. Qi, J. Chen, K. Guo, S. Y. He, J. Yang, Z. L. Li, J. J. Xing, J. F. Hu, H. J. Luo, W. Q. Zhang and J. Luo, *Chem. Eng. J.*, 2019, **374**, 494.
26 K. Zhao, A. B. Blichfeld, H. Chen, Q. F. Song, T. S. Zhang, C. X. Zhu, D. D. Ren, R. Hanus, P. F. Qiu, B. B. Iversen, F. F. Xu, G. F. Snyder, X. Shi and L. D. Chen, *Chem. Mater.*, 2017, **29**, 6367.
27 Y. He, T. Day, T. Zhang, H. L. Liu, X. Shi, L. D. Chen and G. J. Snyder, *Adv. Mater.*, 2014, **26**, 00515.
28 T. Wang, H. Y. Chen, P. F. Qiu, X. Shi and L. D. Chen, *J. Phys.*, 2019, **68**, 18.
29 D. Li, J. H. Zhang, J. M. Li, J. Zhang and X. Y. Qin, *Mater. Chem. Front.*, 2020, **4**, 875.
30 S. Ballikaya, H. Chi, J. R. Salvador and C. Uher, *J. Mater. Chem. A*, 2013, **1**, 12478.
31 Y. Z. Pei, N. A. Heinz and G. J. Snyder, *J. Mater. Chem.*, 2011, **21**, 18256.
32 X. C. Shen, C. C. Yang, Y. M. Liu, G. W. Wang, H. Tan, Y. H. Tung, G. Y. Wang, X. Lu, J. He and X. Y. Zhou, *ACS Appl. Mater. Interfaces*, 2019, **11**, 2168.
33 S. Lin, W. Li, Z. Bu, B. Gao, J. Li and Y. Pei, *Mater. Today Phys.*, 2018, **6**, 60.
34 S. Q. Lin, W. Li, S. S. Li, X. Y. Zhang, Z. W. Chen, Y. D. Xu, Y. Chen and Y. Z. Pei, *Joule*, 2017, **1**, 1.
35 S. Q. Lin, W. Li, Z. L. Bu, B. Shan and Y. Z. Pei, *ACS Appl. Energy Mater.*, 2020, **3**, 1892.
36 H. L. Liu, X. Shi, F. F. Xu, L. L. Zhang, W. Q. Zhang, L. D. Chen, Q. Li, C. Uher, T. Day and G. J. Snyder, *Nat. Mater.*, 2012, **11**, 422–425.
37 X. C. Shen, Y. Xia, C. C. Yang, Z. Zhang, S. L. Li, Y. H. Tung, A. Benton, X. Zhang, X. Lu, G. Y. Wang, J. He and X. Y. Zhou, *Adv. Funct. Mater.*, 2020, **30**, 2000526.
38 O. I. Shpotyuk, M. M. Vakiv, M. V. Shpotyuk and S. A. Kozyukhin, *Semicond. Phys., Quantum Electron. Optoelectron.*, 2017, **20**, 26.
39 X. X. Wang, C. Y. Liu, J. L. Chen, L. Miao, S. H. Wu, X. Y. Wang, Z. C. Xie, W. J. Xu and Q. F. Chen, *CrystEngComm*, 2020, **22**, 248.
40 L. Li, Y. Liu, J. Y. Dai, A. J. Hong, M. Zeng, Z. B. Yan, J. Xu, D. Zhang, D. Shan, S. l. Liu, Z. F. Ren and J. M. Liu, *J. Mater. Chem. C*, 2016, **4**, 24.
41 Y. T. Qiu, J. Yang, D. Y. Wang, M. J. Guan, W. K. He, S. Peng, R. H. Liu, X. Gao and L. D. Zhao, *J. Mater. Chem. A*, 2019, **7**, 26393.
42 H. W. Deng, Z. M. Xie, M. M. Wang, Y. Chen, R. Liu, J. F. Wang, T. Zhang, X. P. Wang, Q. F. Fang, C. S. Liu and Y. Xiong, *Mater. Sci. Eng., A*, 2020, **774**, 138925.
43 R. H. Liu, H. Y. Chen, K. P. Zhao, Y. T. Qin, B. B. Jiang, T. S. Zhang, G. Sha, X. Shi, C. Uher, W. Q. Zhang and L. D. Chen, *Adv. Mater.*, 2017, **2**, 712.
44 C. M. Rost, E. Sachet, T. Borman, A. Moballegh, E. C. Dickey, D. Hou, J. L. Jones, S. Curtarolo and J. Maria, *Nat. Commun.*, 2015, **6**, 8485.
45 R. Chen, P. F. Qiu, B. B. Jiang, P. Hu, Y. M. Zhang, J. Yang, D. D. Ren, X. Shi and L. D. Chen, *J. Mater. Chem. A*, 2018, **6**, 6493.
46 B. Jiang, P. Qiu, H. Chen, J. Huang, T. Mao, Y. Wang, Q. Song, D. Ren, X. Shi and L. Chen, *Mater. Today Phys.*, 2018, **5**, 20.
47 G. D. Tang, F. Xu, Y. He, L. Y. Wang, L. Qiu and Z. H. Wang, *Phys. Status Solidi B*, 2013, **7**, 1327.
48 Z. W. Huang, S. A. Miller, B. H. Ge, M. T. Yan, S. Anand, T. Wu, P. F. Nan, Y. H. Zhu, W. Zhuang, G. J. Snyder, P. Jiang and X. H. Bao, *Angew. Chem.*, 2017, **8**, 134.
49 L. J. Lin, J. H. Wernick, N. Tabatabaie, G. W. Hull and B. Meagher, *Appl. Phys. Lett.*, 1987, **51**, 2051.
50 S. Acharya, J. Pandey and A. Soni, *ACS Appl. Energy Mater.*, 2018, **2**, 1.
51 J. L. Cui, Y. F. Lu, S. P. Chen, X. L. Liu and Z. L. Du, *RSC Adv.*, 2018, **8**, 9574.
52 M. Li, Y. Luo, G. M. Cai, X. Li, X. Y. Li, Z. K. Han, X. Y. Lin, D. Sarker and J. L. Cui, *J. Mater. Chem. A*, 2019, **7**, 2360.
53 X. Yan, G. Joshi, W. Liu, Y. Lan, H. Wang, S. Lee, J. W. Simonson, S. J. Poon, T. M. Tritt, G. Chen and Z. F. Ren, *Nano Lett.*, 2011, **11**, 556.
54 D. B. Zhang, H. Z. Li, B. P. Zhang, D. D. Liang and M. Xia, *RSC Adv.*, 2017, **7**, 10855.
55 G. J. Snyder and E. S. Toberer, *Nat. Mater.*, 2008, **7**, 105.
56 Z. H. Hou, Y. Xiao and L. D. Zhao, *Nanoscale*, 2020, **12**, 026498.
57 W. Li, S. Q. Lin, M. Weiss, Z. W. Chen, J. Li, Y. D. Xu, W. G. Zeier and Y. Z. Pei, *Adv. Energy Mater.*, 2018, **8**, 1800030.
58 T. J. Zhu, S. N. Zhang, S. H. Yang and X. B. Zhao, *Phys. Status Solidi RRL*, 2010, **11**, 317.
59 K. Kurosaki, A. Kosuga, H. Muta, M. Uno and S. Yamanaka, *Appl. Phys. Lett.*, 2005, **87**, 061919.
60 A. Charoenphakdee, K. Kurosaki, H. Muta, M. Uno and S. Yamanaka, *Phys. Status Solidi RRL*, 2008, **2**, 65.
61 F. Reissig, B. Heep, M. Panthfer, M. Wood, S. Anand, G. J. Snyder and W. Tremel, *Dalton Trans.*, 2019, **48**, 15822.

62 S. Ballikaya, H. Chi, J. R. Salvador and C. Uher, *J. Mater. Chem. A*, 2013, **1**, 12478.
63 H. Liu, X. Yuan, P. Lu, X. Shi, F. F. Xu, Y. He, Y. S. Tang, S. Q. Bai, W. Q. Zhang, L. D. Chen, Y. Lin, L. Shi, H. Lin, X. Y. Gao, X. M. Zhang, H. Chi and C. Uher, *Adv. Mater.*, 2013, **25**, 6607.
64 Z. X. Ye, J. Y. Cho, M. M. Tessema, J. R. Salvador, R. A. Waldo, H. Wang and W. Cai, *J. Solid State Chem.*, 2013, **201**, 262.
65 I. S. Osypyshyn, N. V. Chekailo and V. I. Vsesoyuzn, *Physics and Technical Applications of Chalcogenides*, 1988, vol. 3, p. 282.
66 A. Yusufu, K. Kurosaki, Y. Ohishi, H. Muta and S. Yamanaka, *Jpn. J. Appl. Phys.*, 2013, **52**, 81801.
67 D. T. Morelli and G. A. Slack, *High Therm. Conduct. Mater.*, 2006, **2**, 37.
68 J. Krez, J. Schmitt, G. J. Snyder, C. Felser, W. Hermes and M. Schwind, *J. Mater. Chem. A*, 2014, **2**, 13513.